International Journal of Computing and Digital Systems
ISSN (2310-142X)
Int. J. Com. Dig. Sys. 16, No.1 (Jul-24)

http://dx.doi.org/10.12785/ijcds/160108

Improvement in Depth–of–Return-Loss & Augmentation of Gain-bandwidth with Defected Ground Structure For Low Cost Single Element *mm*–Wave Antenna

Simerpreet Singh[1], Gaurav Sethi[1] and Jaspal Singh Khinda[2]

[1]*Department of Electronics and Electrical Engineering, Lovely Professional University, Phagwara, Punjab, India*
[2]*Department of Electrical Engineering, Bhai Gurdas Institute of Engineering and Technology, Sangrur, Punjab, India*

Received 23 May. 2023, Revised 2 Feb. 2024, Accepted 6 Apr. 2024, Published 1 Jul. 2024

Abstract: The present research involves the design, fabrication & testing of a low-cost wide-band *mm*-Wave prototype antenna. The FR4 structure was composed of a Defective Ground Structure (DGS), a Concentric Circle at the bottom edges, and a Rectangular Radiating Patch (RRP) etched with a circle. To improve gain for a wider spectrum, the DGS is created by etching a dumbbell in the center and two semi-elliptical slots at the upper edges. 3.89 GHz (30.26–34.15 GHz) is found to have a bandwidth of -10 dB, and 99% power is obtained with a mismatch loss of less than 0.044 dB for the 30-31.59 GHz band. Additionally, it has a 5–dBi enormous gain-bandwidth of 2.50 GHz (30.47–32.97GHz) & a 3–dBi gain-bandwidth of 3.89 GHz (30.26–34.15GHz). Furthermore, four gain peaks are attained: 9.83 dBi at 31.3 GHz, 8.15 dBi at 32.64 GHz, 6.16 dBi at 33.47 GHz, and 6.05 at 33.74 GHz. Axial ratio, group delay, and directivity are a few more quality metrics that are examined. Anechoic chamber and Rohde & Schwarz ZNB 40 Vector Network Analyzer (VNA) Bench are used to measure antenna parameters. The constructed framework is appropriate for 5G and beyond intelligent network based next-generation (5G) communications, as well as 5G Local Multipoint Distribution Services (LMDS) applications in the *mm*–Wave range and futuristic robotic control devices. Lastly, an equivalent circuit for the suggested structure is created and examined.

Keywords: Concentric circle, K_a–band, Semi-elliptical, *mm*–Wave, Dumbbell

1. Introduction

Due to the development of high-speed, futuristic applications, the need for a wider bandwidth in the communication area has increased tremendously throughout the past ten years. As a result, there is significant frequency congestion at lower spectrum levels. Therefore, in order to prevent interference within the current spectrum, the World Radio Communications (WRC-19) & Federal Communication Commission (FCC) [1], [2] have jointly suggested a new spectrum of 24–42.5GHz in lower *mm*-–Wave range for 5G and beyond [3] communications. In highly populated locations, this broader spectrum can be easily applied to a range of futuristic uses. These could include unmanned robotic machines, Internet of Things (IoT) [1], [4], and Local Multi-point Distribution Services (LMDS). Nevertheless, the substantial transmission losses of *mm*-Wave communication systems limit the signals for short-range and indoor systems. Reducing the mismatch loss (ML_{dB}) as much as feasible can help counterbalance this [5]. The reflection coefficient (S_{11}) is directly related to the mismatch losses [6], which can be decreased to a minimum value of 0.044 dB, that corresponds to $S_{11} \leq$ -20 dB. Six elliptical grooves were etched into the ground plane, increasing the vertical component of current and bringing the mismatch loss down to less than 0.044 dB [7]. Furthermore, the best substrates required to minimize these losses play a crucial role in antenna design for the attainment of intended results. In order to reduce losses, thorough study is being conducted on substrate material selection. Thus, a number of antennas with various substrates have been reported before [8], [9], [10], [11], [12], [13], [14], [15], [16], [17], [18].

A *mm*–Wave MIMO antenna with a peak–gain of 9.08 dBi & a bandwidth of 30–40GHz was presented by Wadhwa et al. (2022) [8]. It was structured on the inexpensive material FR4. Despite having a higher bandwidth, the 1 × 4 MIMO design makes the antenna more complex and bulkier in size. In order to attain *mm*–Wave range, Hu et al. (2021) [9] studied SIW feeding based wideband filtering antenna. The antenna is built upon many layered Rogers 3001, Rogers COOLSPAN, and RT/Duroid 5880 substrates. By adding nulls between interfering directions, Hu et al. (2016) [10] created a 64-element array (antenna) on a Low Temperature Co–fired Ceramic (LTCC) substrate to increase signal to noise ratio. These antennas are difficult to construct, expensive, and feature complex array designs [9], [10]. The MIMO antenna on a flexible substrate, such as Poly Ethylene Terephthalate (PET), was presented by Jilani et al. (2018) [11] for wearable *mm*–Wave applications based on switchable approaches. A beam steering end firing *mm*–Wave Planar Inverted F–Antenna (PIFA) with anti-reflective layer technology

E-mail address: s.simerpreet@gmail.com, gaurav.11106@lpu.co.in, jskhinda@gmail.com

and grating strip was developed by Taheri et al. (2019) [12]. The Nelco N9000 substrate, measuring 70 × 120 mm^2, is used for its design. The suggested design's array structure increases its size and renders it incompatible with the Ultra Large Scale Integrated (ULSI) chipsets that are available today. An array in the partial *mm*–Wave range with a peak–gain of 3.8 dBi at 30.5GHz was introduced by Liu et al. (2017) [13]. For 5G applications, a large 8 × 4 phased array module with many concurrent beams is made possible by the antenna structure, which is settled on intricate organic layered substrates made of copper substrate & supports both horizontal & vertical polarization. In the Mantash & Denidni [14], a ring-shaped wearable antenna was provided with a moderately priced copper substrate, and several performance matrices were examined. The extracted gain bandwidth, which had an overall bandwidth of 25–35GHz and a peak gain of 5.5 dB, was 28–33GHz. Flexible wearable gadgets can be integrated with these futuristic antennas. A single element *mm*–Wave antenna with a dimension of 10 × 12 mm^2 constructed on FR4 substrate was presented by Singh et al. (2022) [15]. Despite its small size and extremely low manufacturing cost, the antenna has a limited bandwidth of 36.25–38.25 MHz in the *mm–wave* range. Alsudani et al. (2023) designed a compact 7.24 × 6.24 mm^2 *mm*–Wave antenna [16] using an expensive Roger RO3003 substrate. With a maximal gain of 6.48dBi, the antenna's resonance frequency is limited to 28 GHz. Larger antennas are a result of a meta-surface [17], array/MIMO/frequency selective surface (FSS) [18], and complicated designs with extremely low 5-dBi-fractional-gain-and impedance-bandwidths.

From the above discussions, it can be concluded that the state-of-the-art prototypes [8], [9], [10], [11], [12], [13], [14], [15], [16], [17], [18] and narrow impedance–and gain–bandwidth in *mm*–Wave range were all plagued by the same weakness. Another significant barrier to its practical interoperability with ULSI small communication systems is the larger array/MIMO prototypes. Furthermore, because of their -20 dB constrained bandwidth, the majority of these prototypes had a very limited spectrum of lower admissible mismatch loss, or less than 0.044 dB. As a result, the source can only supply 99% power for a short period of time at a few MHz to patch. Furthermore, the inclusion of pricey substrates like RT/Duroid 5880, LTCC, PET, Nelco N9000, Copper, Roger RO3003, and others in the design of the prototypes mentioned raises the cost of communication equipment. In order to get over the previously mentioned restrictions, a unique single element DGS antenna is constructed using an affordable FR4 substrate. The broader bandwidth of 3.89 GHz (30.26–34.15 GHz) and 3–dBi gain bandwidth of 3.89 GHz (30.26–34.15 GHz) are achieved by the suggested antenna design, with a peak gain of 9.83 dBi at 31.30 GHz. Additionally, it provides a 5–dBi-gain-bandwidth of 2.50 GHz (30.47–32.97GHz) and a wide band of 1.59 GHz (30–31.59GHz) with mismatch loss smaller than 0.044 dB, ensuring 99% power delivery to patch from its exciting source for the aforementioned larger spectrum. Combination etchings of dumbbell in ground plane and concentric circles in patch increase the gain and bandwidth. With its low hardware cost, wide bandwidth, low mismatch loss, high peak gain, and larger 5-dBi-gain-bandwidth, the suggested antenna is a good fit for future machine applications and LMDS (31–31.3GHz).

2. Design Methodology

Figure 1 illustrates the suggested *mm*–Wave antenna structured on FR4 substrate with dimensions of 27.5 × 20 × 1.6 mm^3. It consists of a rectangular patch measuring 15 × 20 mm^2 that has been etched with three circles with radii of r_1 = 2 *mm*, r_2 = 4 *mm* & r_3 = 6 *mm* respectively called C_1, C_2, & C_3. To create the concentric circle known as C_{23}, the circle C_2 is trimmed away from C_3. To obtain the final antenna patch (P) configuration, a small circle C_1 & concentric circle C_{23} are etched in the RRP. Additionally, a rectangular slit is etched horizontally between the feeding position to the patch (P) and the concentric circles C_{23}.

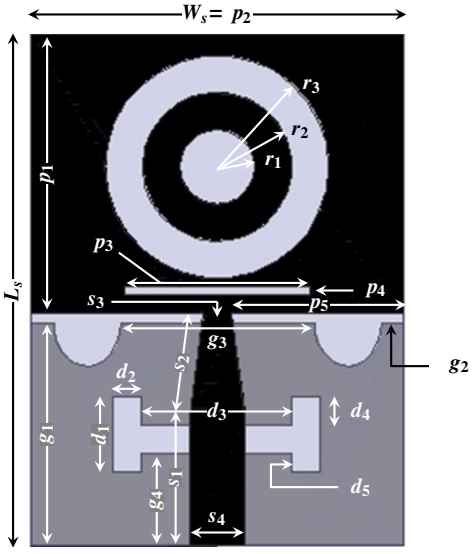

Figure 1. The concentric circle antenna parameters; L_s = 27.5, W_s = 20, p_1 = 15, p_2 = 20, p_3 = 10, p_4 = 0.5, p_5 = 8.5, r_1 = 2, r_2 = 4, r_3 = 6, g_1 = 12, g_2 = 1.2, g_3 = 10.4, g_4, s_1 = 7, s_2 = 5.55, s_3 = 1.5, s_4 = 3, d_1 = 4, d_2 = 1.5, d_3 = 8.1, d_4 = 1.5, d_5 = 1. (all in *mm*)

An ohmic contact is established between the microstrip feeding line (F) and the patch P to enable impedance matching. The GP is positioned with its outside dimensions of 12 × 20 mm^2 on the back side of the RP and FR4 substrate. With a main radius of 1.8 *mm* & an elliptical ratio = 1.3, the upper corners of the rectangular GP are chopped off semi-elliptically. Additionally, GP has a dumbbell-shaped slot etched in the middle, which leads to the ultimate development of DGS. The final microstrip antenna design for the *mm*–Wave range is configured in a concentric circular shape thanks to the combination of patch P, DGS, and feeding line 'F'.

3. Equivalent Circuit of Antenna configuration.

For RF input, a 50 Ω excitation port is utilized. A 50 Ω feed-line having width = 3 *mm* is represented by an inductor and capacitor combination in series. A 5.5 mm impedance transformer tapered portion matches the

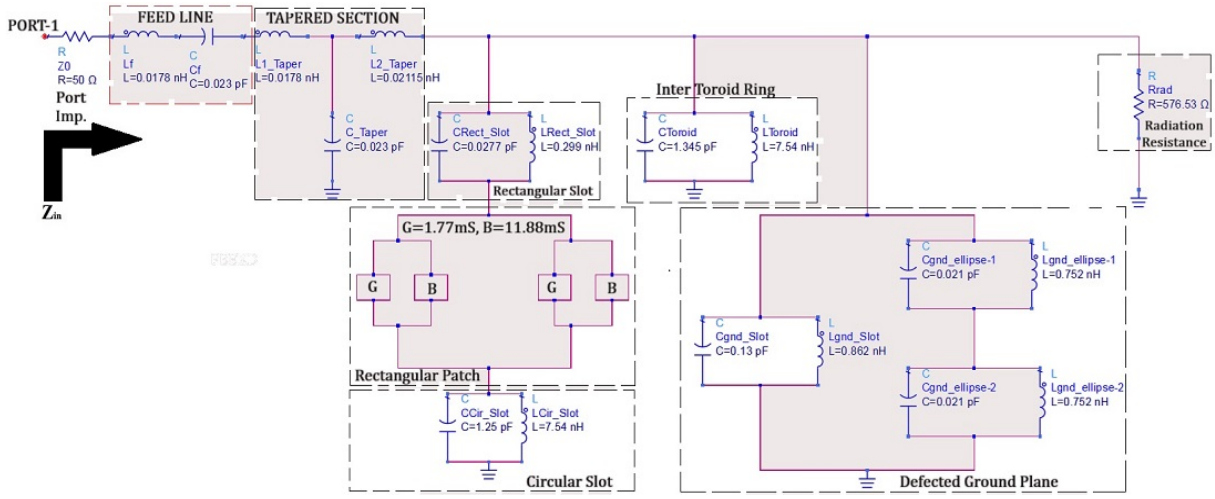

Figure 2. The equivalent circuit of antenna configuration.

TABLE I. Passive component values of the concentric circle antenna configuration.

Section Name	Sub-section Name	Parameter Name	Parameter Values
Port	none	Port Impedance	$Z_0 = 50\Omega$
Feed Line	none	Feed Inductor	$L_f = 0.0297nH$
		Feed Capacitor	$C_f = 0.511\ pF$
Tapered section	none	Taper Inductor Sec.-1	$L_{1Taper} = 0.0178\ nH$
		Taper Inductor Sec.-2	$L_{1Taper} = 0.02115\ nH$
		Feed Capacitor	$C_{Taper} = 0.023\ pF$
Slotted Rectangular Patch	Rectangular Slot	Rect. Slot Inductor	$L_{Rect.slot} = 0.299\ nH$
		Rect. Slot Capacitor	$C_{Rect.slot} = 0.0277\ pF$
	Rectangular Patch	Conductance sec.-1	$G = 1.77\ mS$
		Susceptance sec.-1	$B = 11.88\ mS$
		Conductance sec.-2	$G = 1.77\ mS$
		Susceptance sec.-2	$B = 11.88\ mS$
	Circular Slot	Cir. Slot Inductor	$L_{Circ.-slot} = 7.54\ nH$
		Cir. Slot Capacitor	$C_{Circ.-slot} = 1.25\ pF$
	Inner Toroid Ring	Cir. Slot Inductor	$L_{Toroid} = 5.0267\ nH$
		Cir. Slot Capacitor	$C_{Toroid} = 1.345\ pF$
Defected Ground Plane	Slot	Gnd Slot Inductor	$L_{gnd.-slot} = 0.862\ nH$
		Gnd Slot Capacitor	$C_{gnd.-Slot} = 0.13\ nH$
	Ellipse slots	Inductor ground ellipse-1	$L_{gnd.-elipse-1} = 0.752\ nH$
			$L_{gnd.-elipse-2} = 0.752\ nH$
		Inductor ground ellipse-2	$C_{gnd.-elipse-1} = 0.021\ pF$
			$C_{gnd.-elipse-2} = 0.021\ pF$
Radiation	none	Radiation Res.	$R_{rad.} = 576.53\ \Omega$

impedance of the 50 Ω feed line with the slotted rectangular patch. An comparable T–section represents this tapered section [19], [20]. An outside circle with a radius of 6 mm, an inner concentric circle with an average radius = 3 *mm* & a width = 2 *mm* and a rectangular slot measuring 0.5 mm × 10 mm make up a rectangular patch. According to Balanis (2016) and Kai (2015), the rectangular patch is depicted as a parallel combination of equal conductance and susceptance (G + jB) on either side of the feed line. LC-tank circuits are a representation of the two routes that a rectangular and circular slot divides the current into [21], [22]. Charge builds up significantly close to the outer circle. It is also referred to as an LC-tank circuit and has a concentric circle ring at the center of the outer circle that increases the radiations brought on by displacement current [21].

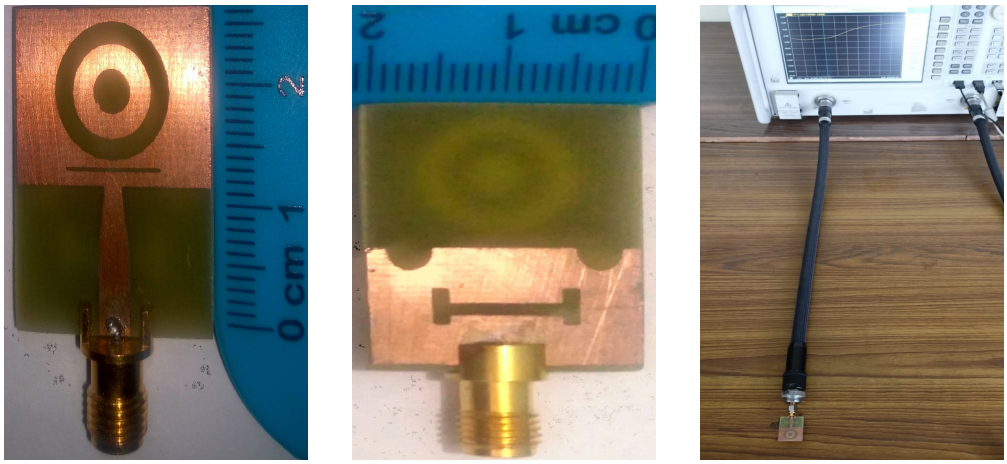

(a) (b) (c)

Figure 3. The fabricated antenna structure a) Front view b) Back view c) Antenna testing setup using VNA

Two semi-elliptical incisions and a symmetrical hybrid rectangular slot make up the ground. The ground surface current is split into two routes by a hybrid rectangular slot, which subsequently combines them. As a result, an LC parallel network is another representation of it [21]. Extra charges are stored in two semi-elliptical truncated ground corners, which also improve the ground width's perimeter. Consequently, a combination of an inductor and a capacitor is used to represent these. There is an inductor because of the increase in the periphery and a capacitor because of the accumulation of surplus charge [21]. The R_{rad} represents the total radiation resistance. Table I displays all of the calculated parameters, and Figure 2 depicts a *RLC* electrical equivalent circuit that corresponds to the geometrical structure.

Significance of Equivalent Circuit: The primary benefit of doing such an in-depth study is that, since embedded/low power VLSI systems are the most common, the researchers may integrate any planar or three-dimensional antenna operating in the microwave frequency band.

4. Fabricated Prototype and Testing

The prototype of the suggested structure and its testing setup with the Rohde & Schwarz ZNB 40 (100 KHz–40GHz) Vector Network Analyzer is illustrated in Figure 3. For excitation purposes, a unique 2.92 mm (female) end launch co–axial connector with an impedance = 50 Ω is connected to the end of feeding-line.

The step by step procedure to fabricate this prototype is illustrated below.

Chemical-Etching: - In this kind of procedure, a very tiny layer of material is produced on substrate by treating it with a material that has photo resistance properties with the use of an air brushing technique. In order to increase the homogeneity level that air brushing cannot, the spinner method is also employed. It is imperative that the coating level be kept between 1.5 and 2 microns [4]. The coated board is heated to 100^0C for a brief period of time (1-2 minutes) following the spinning operation in order to dry it off. The .dxf file of the antenna geometries are drawn to board and exposed to UV light for approximately two to three minutes in order to remove the photo resist. Following a thorough cleaning and drying process, the substrate board is placed in the $FeCl_3$ (ferric chloride) solution to begin the etching process. The final step in removing any remaining photoresist material or contaminants is acetone rinsing [4].

Photo-Lithography: - The design created using computer–aided software is the foundation of this procedure. The geometries of antenna are designed & the see-through sheet is published with reverse masking, also known as negative masking. Nowadays, great attention is taken in selecting the substrate with copper metallization and an etched patch [4]. A thin coating of image-resist solution with thinner is applied & coated on Cu (Copper) planes in this process as well, following the first cleaning with acetone. Again, because it allows for thinner deposition, spinning method is recommended here. Once it has completely dried, the photo resist material is covered with the mask and exposed to UV light, which solidifies the material. Next, a dye solution is applied to the substrate, revealing photoresist sections on the coating. To remove any undesired deposits, it is once more cleaned using acetone and $FeCl_3$.

Co–ordinatograph (based on computer):- This software application which is essentially CAD–based, is utilized to create the antenna geometry design system's mask. To visualize the saved antenna geometry, a gerber file is created, and a photo-plotter is utilized to design the mask. This mask is an exact replica of intended geometrical design & it is utilized once more for substrate etching. a broad view of the manufactured substrate.

Antenna-Testing:- Verification of results [4] and simulated design of antenna geometry are carried out

through testing. Research potential is tested using Network Analyzer (NA). The S–parameters are typically measured at very high frequencies since they are easier to compute using a network analyzer [4]. It functions in the time and frequency domains. Microwave research laboratories use it to observe how antenna-based devices, mixers & filters react at these high radio frequencies. The response of antenna on NA is used to fix or characterize it for its application based system & to uncover the produced antenna's performances. A variety of measurement qualities lead to the universal use of three different types of NAs. Since it lacks a vector element, the Scaler Network Analyzer, or SNA, is the most basic type of network analyzer and is used to observe the scaler features of antennas and other microwave radiating devices. This kind of analyzer has a tracking generator and spectrum analyzer functions. The tracking generator's output terminal serves as the spectrum analyzer's input terminal because it generates a sweeping signal with a frequency level that is comparable to that of the analyzer. The spectrum analyzer illustrates the response of amplitude in relation to the frequency alteration. As its name suggests, the VNA is a more potent & useful network analyzer than the SNA because, in addition to measuring vector elements like amplitude and phase, it can also measure scalers. As a result, it can also provide the gain level; for this reason, it is also referred to as a gain–phase meter. It offers best information possible on antenna and other device designs for optimal performance. The Large Scale Network Analyzer, or LSNA, is intended for devices that rely on extremely high level signal conditions. It offers a thorough perspective that takes into account the device's nonlinear behavior and harmonics. This analyzer, often called a microwave transition analyzer, is typically used for devices that are based on microwave frequencies.

5. Results and Discussions

The proposed concentric circle antenna configuration's computed and noticed reflection co-efficient (S_{11}) is demonstrated in Figure 4. The figure illustrates that a -10 dB impedance bandwidth in the mm–wave range can be obtained at 3.89 GHz (30.26–34.15 GHz). Additionally, it attains a bandwidth of 1.59 GHz (30-31.59 GHz) with impedance of -20 dB, ensuring 99% power transfer from the source to the patch. This results in a very low mismatch loss ≤ 0.044 dB for the given bandwidth, resulting in decreased reflections. In addition, a resonance frequency of 30.45 GHz and a corresponding S_{11} = -24.63 dB are noted for the antenna.

Plots exhibiting the gain for the proposed concentric circle antenna configuration are presented in Figure 5. A broad 3-dBi gain bandwidth of 3.89 GHz (30.26–34.15 GHz) has been found to be attained. At frequency 31.30 GHz, a peak-gain of 9.83 dBi is likewise noted, and S_{11} corresponds to a value of -22.57 dB. These data readily lead to the conclusion that the proposed antenna configuration offers a maximum gain = 9.83 dBi along with a mismatch loss ≤ 0.044 dB and a power delivery to the patch of 99% from the source. Three further gain peaks are detected, corresponding to 8.15 dBi at 32.64 GHz, 6.16 dBi at 33.5 GHz, and 6.05 dBi at 33.74 GHz. A narrow bandwidth of 31 MHz (32.97-33.28GHz) is excluded from the design, which also includes the 5-dBi gain-bandwidth of 3.47 GHz (30.47-33.94GHz). There is acceptable agreement between the simulated and measured S_{11} & gain-plot results. The discrepancy between their values are caused by practical and ideal environmental conditions. As a result, this device is practically useful for Ka-band, flexible wireless devices, and upcoming 5G applications. Figure 6 illustrates the directivity and VSWR plots of the proposed concentric circle antenna arrangement. Directivity is demonstrated to follow the gain-plot curve, however its values are greater than the gain values in the frequency range of the mm–Wave spectrum. At 31.30 GHz, the highest directivity value of 12.76 dB is achieved. Furthermore, as can be seen on the right y-axis of Figure 6, the VSWR is still less than 2.

With respect to frequency, the mismatch loss (dB) on the left y-axis and the power (%) on the right y-axis

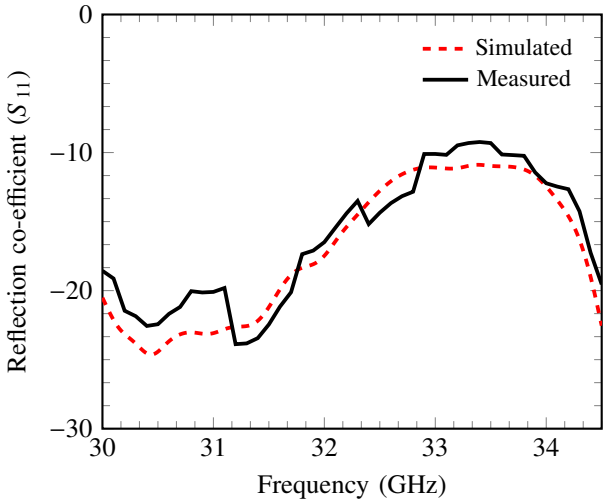

Figure 4. The S_{11}-plots of concentric circle antenna configuration.

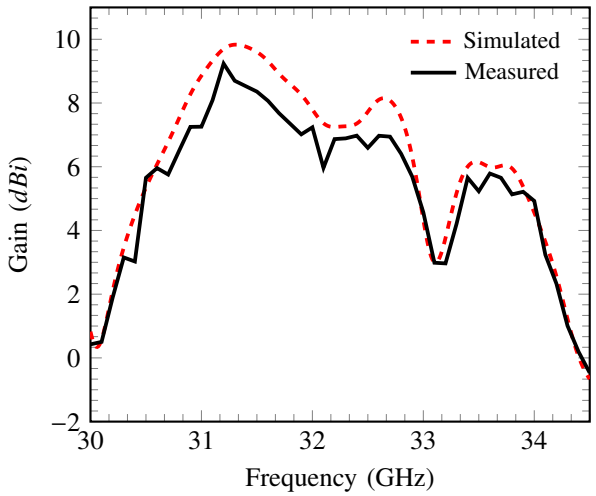

Figure 5. The gain-plots of concentric circle antenna configuration.

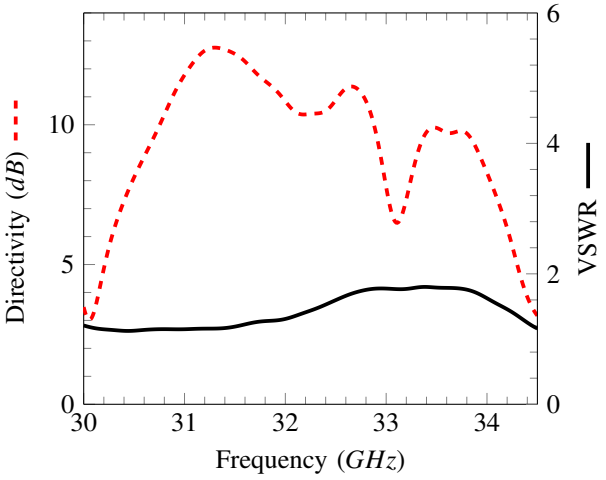

Figure 6. The directivity and VSWR–plots of concentric circle antenna configuration.

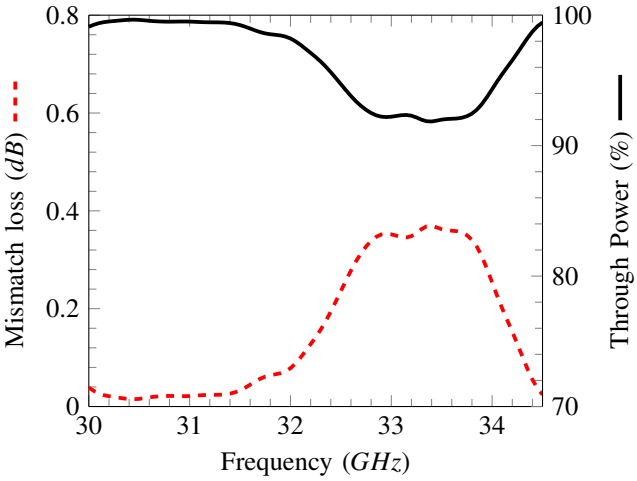

Figure 7. The mismatch loss (dB) and through power (%) of concentric circle antenna configuration.

are demonstrated in Figure 7 and depicted that the corresponding power is larger than 90% and the mismatch loss value stays less than 0.45 dB throughout the full range. Additionally, mismatch loss≤ 0.044 dB bandwidth is detected at 30–31.59GHz, and the resulting through power improves to 99%. This indicates that with a 1.59 GHz bandwidth, 99% of the power is transferred to its destination (patch) from excitation source.

The configuration to determine the antenna's transmission characteristics is illustrated in Figure 8. As depicted in Figure 9, two identical antennas are positioned face to face at a distance (d) = 50 cm & group delay is detected for the desired frequency range. The group delay variation for face-to-face orientation is shown to be extremely small, at 0.7 ns. For the antenna under study, these fluctuations in nanoseconds are regarded as a continuous group delay.

The suggested antenna design's axial ratio is illustrated in Figure 10. Over the whole spectrum, the axial ratio values are seen to be greater than 3 dB. This

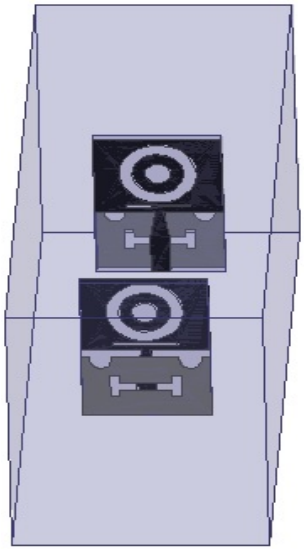

Figure 8. The setup of antenna for calculation of group delay.

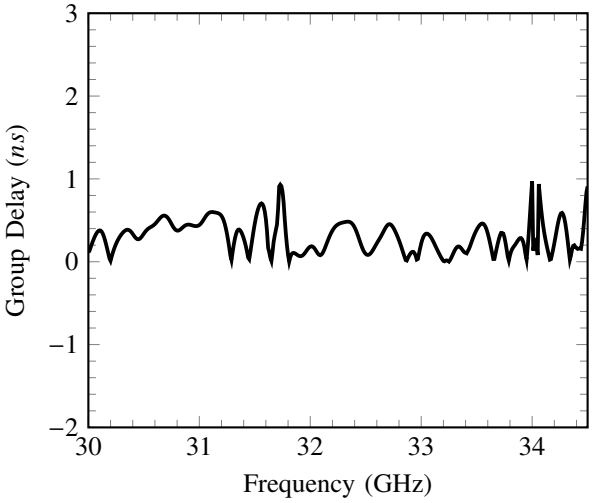

Figure 9. The group delay of the concentric circle antenna configuration.

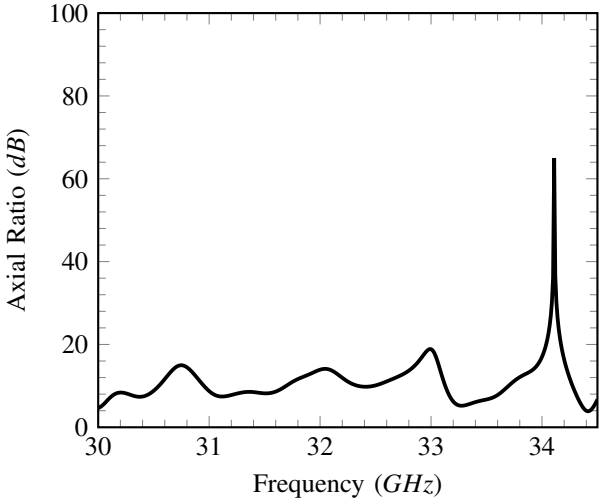

Figure 10. Axial ratio of the concentric circle antenna configuration.

led to the conclusion that the *mm*–Wave antenna's

design is linearly polarized.

A. Stage Evolution

Figure 11 depicts the step-by-step evolution of the proposed concentric circle antenna configuration, which was covered in the preceding section. The antenna's basic design is illustrated in Figure 11 (a), with dimensions determined in accordance with [5]. It consists of a 50 Ω tapered feeding line that feeds a GP measuring 12 × 20 mm^2 and an RP measuring 15 × 20 mm^2. This allows for a smooth flow of current from source to patch.

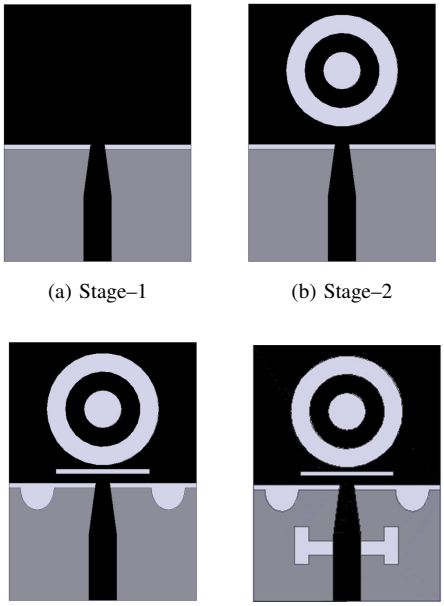

(a) Stage–1 (b) Stage–2

(c) Stage–3 (d) Stage–4

Figure 11. The stage-wise evolution of concentric circle antenna configuration.

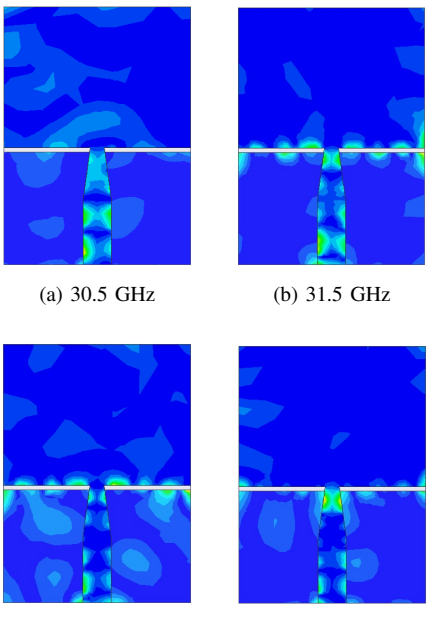

(a) 30.5 GHz (b) 31.5 GHz

(c) 32.5 GHz (d) 33.5 GHz

Figure 12. The electric field distribution of Stage–1.

After analyzing the electric field distribution of Stage-1, illustrated in Figure 12, it is evident that the coupling between GP and RRP is mostly responsible for the uniformity in the electric field distribution. Furthermore, it is discovered that the patch's center does not participate in radiations because of the minimal electric field distribution associated with it. The field is primarily dispersed around the RRP's margins. Therefore, cutting off the middle section concentrically (C_{23}) & with C_1 as previously suggested would not have a substantial impact on the radiation outcomes in Stage-2. This configuration enhances the gain by lowering copper losses, as Figure 17 later demonstrates.

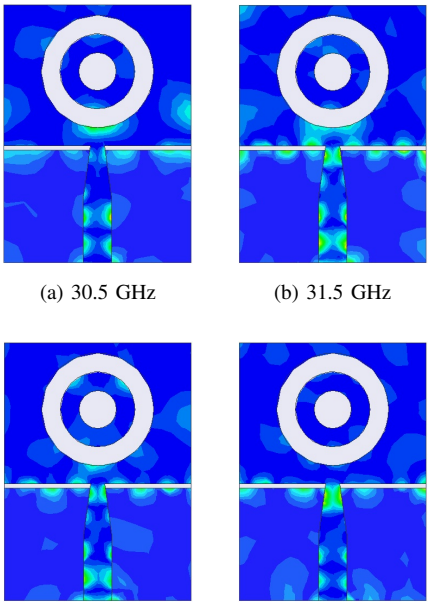

(a) 30.5 GHz (b) 31.5 GHz

(c) 32.5 GHz (d) 33.5 GHz

Figure 13. The electric field distribution of Stage–2.

The electric field distribution of Stage–2 is depicted in Figure 13, and it is noted that the electric field is not evenly distributed across the patch's surface. We find that there is connection in the upper section of GP and the lower part of RRP. In order to decrease capacitive coupling between them, two semi-ellipticals with main radii of 1.8 *mm* and an elliptical ratio of 1.3 *mm*, respectively, are trimmed off from the upper margins of GP, as shown in Figure 14. Additionally, a horizontal slit is carved close to the RRP feeding point in order to spread surface current on Stage 3 of the antenna's RRP results.

The concentric circle antenna configuration's electric field distribution for Stages–3 and Stage–4 is illustrated in Figure 14 and 15, respectively, and it exhibits that the etching of two dumbbells in GP has a considerable impact on the surface current distribution of RRP. In comparison to Stage-3, the consistency of the electric field has significantly improved in Stage-4. As such, it plays a major role in improving gain-bandwidth.

The S_{11}– & gain-plots of Stages-1,-2,-3, and-4 are compared in Figure 16 & 17, respectively. It can be seen

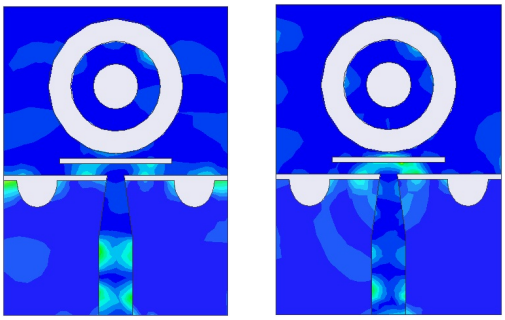

(a) 30.5 GHz (b) 31.5 GHz

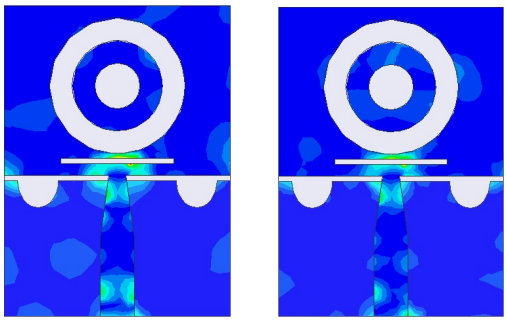

(c) 32.5 GHz (d) 33.5 GHz

Figure 14. The electric field distribution of Stage–3.

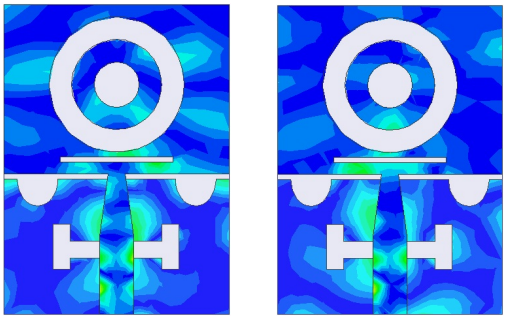

(a) 30.5 GHz (b) 31.5 GHz

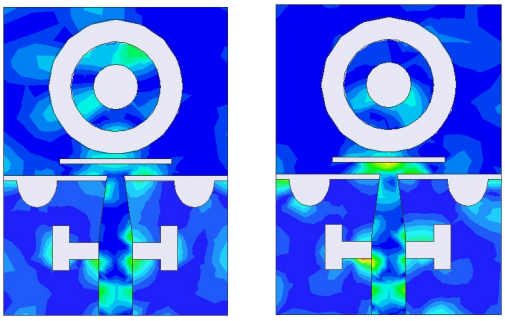

(c) 32.5 GHz (d) 33.5 GHz

Figure 15. The electric field distribution of Stage–4.

that improving the etching of concentric circles in RRP enhances the structure's gain and impedance matching. This improvement in gain is the result of the radiating patch's decreased copper loss.

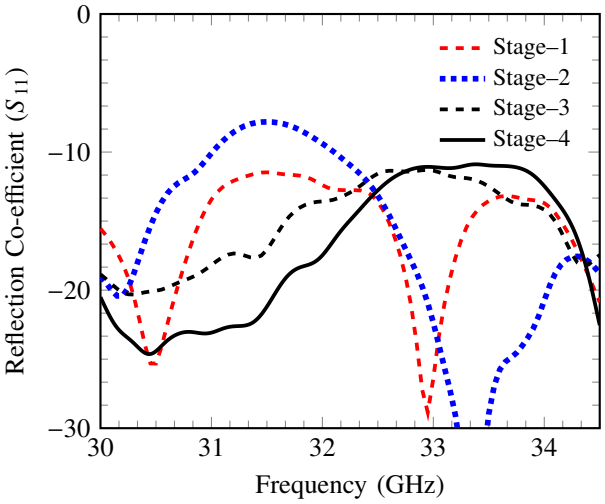

Figure 16. The stage-wise reflection co-efficient of concentric circle antenna configuration.

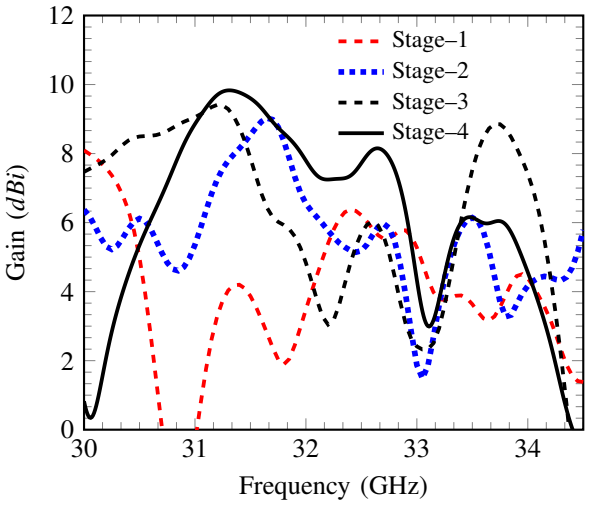

Figure 17. The stage-wise gain–plots of concentric circle antenna configuration.

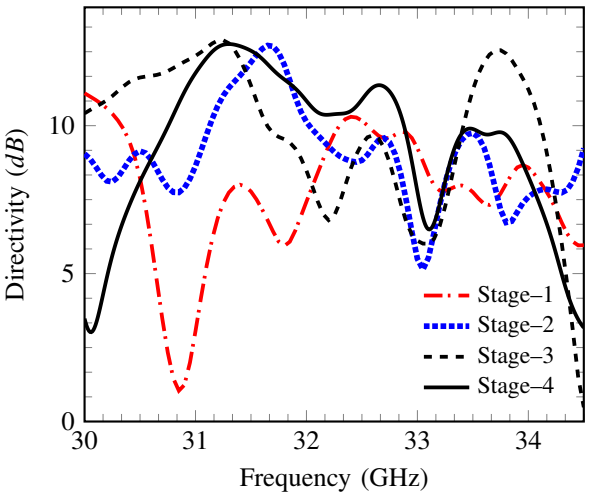

Figure 18. The stage wise directivity–plots of concentric circle antenna.

TABLE II. The comparison of performance parameters for concentric circle antenna configuration at different stages.

	Bandwidth (GHz)		Mismatch Loss (dB)		Gain–Bandwidth (GHz)		Peak–gain	
Stages	**-10 dB**	**Frac. (%)**	**≤ 0.044 dB**	**Frac. (%)**	**5 dBi**	**Frac.(%)**	**(dBi)**	**Freq. (GHz)**
1	30–34.5	13.95	30.28–30.69	1.35	32.16–33.03	2.67	6.37	32.4
2	30–31	3.28	32.91–34.03	3.35	30–30.72	2.37	9.03	31.65
	32.12–34.5	7.15			30.96–32.83	5.86		
3	30-34.5	13.95	30.17–30.52	1.15	30–31.98	6.39	9.41	31.2
					33.34–34.18	2.49		
4	30.26-34.15	12.08	30–31.59	5.16	30.47–33.94	10.77	9.83	31.3
					33.28–33.95	1.99		

Figure 18 illustrates directivity is compared over the four phases. Directivity values can be seen to have significantly improved at each evolutionary step. As exhibited in Table–II, it is also found that peak-gain and peak-directivity can be obtained at the same frequency in all phases.

A stage-by-stage comparison of antenna performance parameters is shown in Table–II. It is simple to conclude that there has been stage-wise improvement in gain-bandwidth, peak-gain, and peak-directivity from Figure 16 to 18 and Table–II. These enhancements result from the etching of different slots in the ground plane (GP) & radiating patch (RRP), in accordance with the electric field distribution studies discussed in Section 5-A.

B. *Parametric study*

Parametric analysis can be used to optimize the antenna performance parameters. The key geometrical and electrical parameters that affect these investigations are the existence of concentric circles, central circles, patch slit lengths, semi-elliptical slot positions, and the length and placement of dumbbells in the ground portion.

1) *Affect of concentric circles (C_{23}) & central circle C_1 on performance parameters*

The patch (P) with one central small C_1 & concentric circle C_{23} is illustrated in Figure 19, and the associated performance parameters are shown in Figure 20. When comparing the S_{11}–plots on the left y–axis, it is evident that the design depicted in Figure 19 (c) has better impedance matching. For all other designs, on the other hand, the value of S_{11} stays less than -10 dB across the frequency of interest. When gain-plots are compared along the right y–axis, it is seen that the gain-plot for Figure 19 (a) is not very attractive. For the structure demonstrated in Figure 19 (d), the optimum 3 dBi gain-plot is obtained.

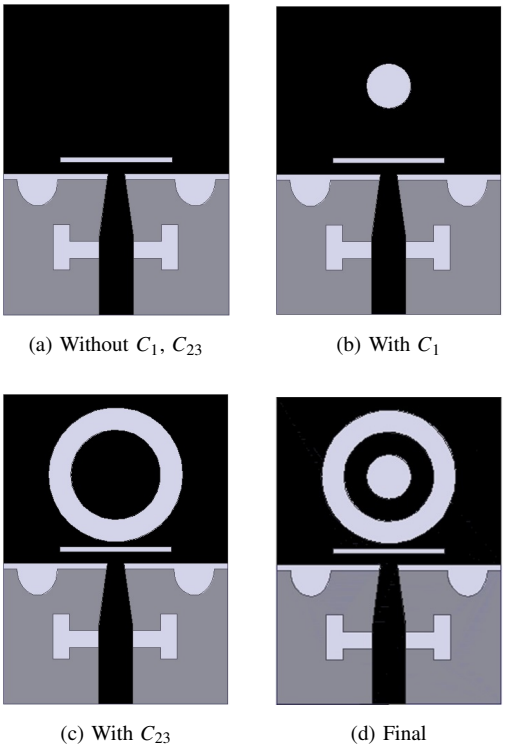

(a) Without C_1, C_{23} (b) With C_1

(c) With C_{23} (d) Final

Figure 19. Antenna configurations with various circle etchings.

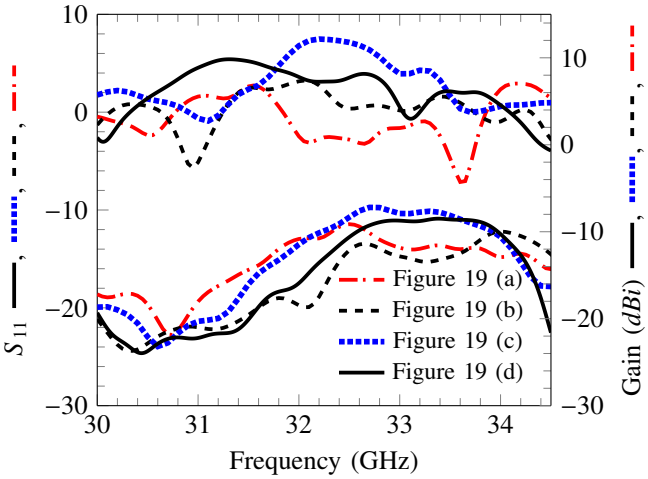

Figure 20. Etchings effect of central small C_1, concentric circle C_{23} on performance parameters.

2) *Affect of patch slit width (p_3)*

It can be shown from Figure 21 that impedance matching deteriorates beyond 32 GHz with an increase in value of p_3. Variations are analyzed at p_3 = 5 *mm*, p_3 = 10 *mm*, and p_3 = 15 *mm*. Furthermore, the gain-plots for p_3 = 5 *mm* and p_3 = 15 *mm* are not very striking.

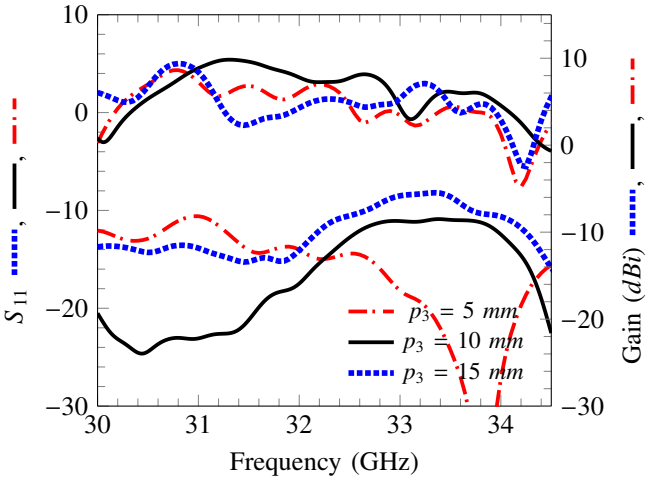

Figure 21. Affect of patch slit length i.e. p_3 = 5 *mm*, p_3 = 10 *mm*, p_3 = 15 *mm* on performance parameters.

3) Affect of dumbbell width (d_3)/position (g_4)

The impact of variations in distance d_3 at 4 *mm*, 8.1 *mm*, and 12 *mm* between the two dumbbells is analyzed in Figure 22. While d_3 = 4 *mm* to d_3 = 12 *mm* is shown

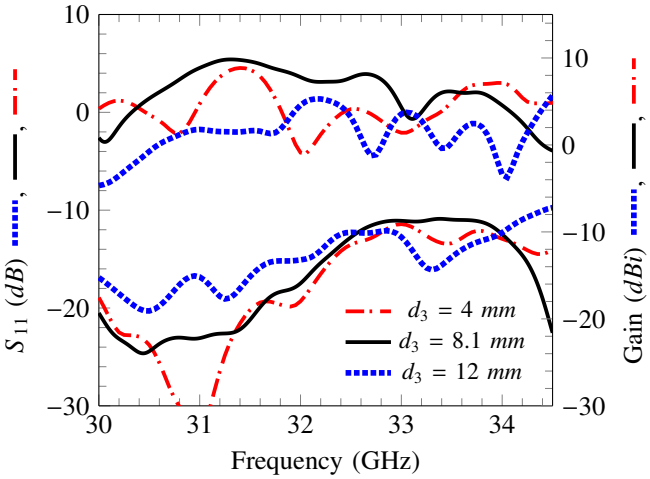

Figure 22. Affect of ground dumbbell length i.e. d_3 = 4 *mm*, d_3 = 8.1 *mm*, d_3 = 12 *mm* on performance parameters.

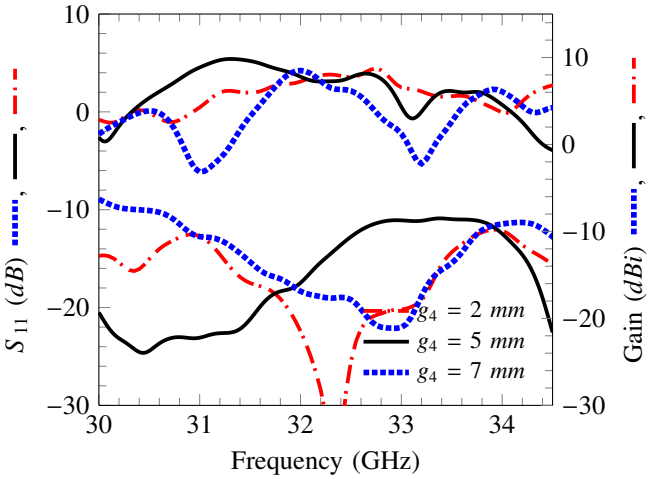

Figure 23. Affect of ground dumbbell length i.e. g_4 = 2 *mm*, g_4 = 5 *mm*, g_4 = 7 *mm* on performance parameters.

to cause S_{11} to decrease, its graphs stay ≤ -10 dB throughout the entire spectrum of interest. Furthermore, it can be seen from the y-axis that there are more unresolved harmonics for d_3 = 4 *mm* and d_3 = 12 *mm*. The impact of dumbbell position on DGS is shown in Figure 23, where it is shown that impedance matching is enhanced over the 31.5–33.5GHz range at g_4 = 2 *mm* & g_4 = 7 *mm* (i.e., dumbbell at extreme position toward its edges). The gain values, however, drastically decline.

4) Affect of distance (i.e. g_3 = 6 mm, g_3 = 10.4 mm & g_3 = 12.4 mm) between ground edge ellipses

The impact of the distance between the edges of the semi-ellipses at g_3 = 6 *mm*, g_3 = 10.4 *mm* & g_3 = 12.4 *mm* on the performance parameters of prototype is illustrated in Figure 24. It is noted that impedance matching deteriorates with increasing distance between the two semi-ellipses, as computed at g_3 = 12.4 *mm* in this case, but improves with decreasing distance (i.e. here g_3 = 6 *mm*). Gain is also calculated for the same values of g_3 in addition to S_{11}, and it is discovered that the best results are attained at g_3 = 10.4 *mm*.

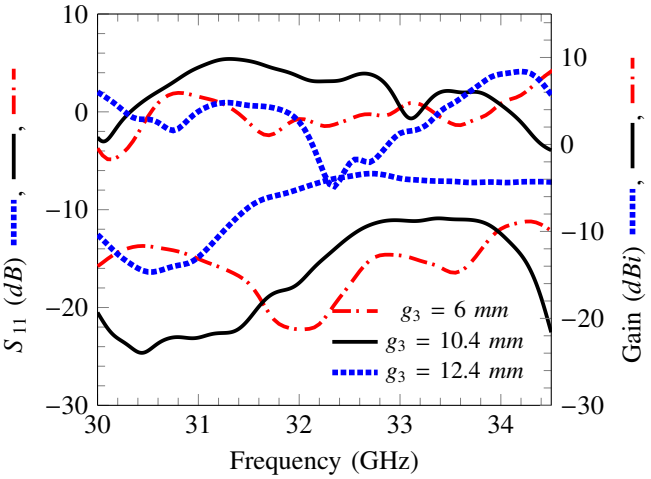

Figure 24. Affect of ground dumbbell length i.e. g_3 = 6 *mm*, g_3 = 10.4 *mm*, g_3 = 12.4 *mm* on performance parameters.

The different characteristics of cutting-edge antennas are compared with suggested research projects in Table III. Related works have shown that they were designed with costly materials, such as LTCC, PET, RT/Duroid 5880, Nelco N9000, Rogers RO3003 and Roger RO4350B which have larger and more sophisticated designs as a result of array/MIMO structures. Furthermore, the high peak gain and larger gain-bandwidth are not covered by these antennas. But because FR4 substrate is used, the single element prototype's peak gain is relatively high, its size is small, and its fabrication is inexpensive. Furthermore, this prototype spanned a low mismatch loss bandwidth of about 1.55 GHz and a broader *mm*–Wave. These performance characteristics, which include a high peak-gain = 9.83*dBi* at 31.3GHz, make it appropriate for use in future robotic control communication devices. LMDS in the 31.0–31.3GHz frequency range can be used for a range of applications, including voice and IP data, to accommodate a high user capacity in densely populated areas.

TABLE III. A comparison between the proposed Concentric Circle antenna specifications and various state-of-the-art *mm*-wave antennas that have been described.

#	Antenna Size (mm^2)	Number of Array Elements	*mm*–Wave						Substrate Used	Design Complexity
			Bandwidth (GHz)	Fractional Bandwidth (%)	Peak-Gain (dBi)	at Freq.	Gain ≥ 5 dBi (GHz)	Mismatch Loss ≤ 0.044 dB		
[8]	37 × 15	1 × 4	30–40	28.57	13.69	29 GHz	30–40	-	FR4	High
[9]	50 × 50	4 × 4	30–31.15	3.76	18.5	30.6 GHz	30-31.5	25.2–28GHz	Duroid 5880	High
[10]	1 × 1.23	1 × 64	36–40	10.53	6.5	37.5 GHz	36–36.3	37.8–38.4GHz	LTCC	High
[11]	11 × 25.4	1 × 2	30–40	28.57	6.2	34 GHz	30-34	32–33.8GHz	PET	High
[12]	70 × 120	1 × 4	30–31	3.28	9	29 GHz	30–31	21.8–22.2GHz	N9000	High
[13]	20 × 20	4 × 16	30–36	18.18	3.8	30.50GHz	30–31.3	30.62–30.8GHz	Copper	High
[14]	20 × 20	Single	30–33	9.52	5.5	29 GHz	30–35	26–31.50GHz	Copper	High
[15]	10 × 12	Single	34.72–40.72	3.70	12.4	35.1 GHz	36.25–38.25	36–38.5GHz	FR4	Low
[16]	7.24 × 6.24	2 × 2	28	Nil	6.48		28 GHz	at 28 GHz	Rogers RO3003	High
[17]	12 × 12	MIMO	23.9–30.7	24.9	9.4	30–32	29 GHz	28–29	Rogers 5880	High
[18]	5.36 × 5.36	Array	32–43.10	29.6	17.65	30–36	29–36	35.5–36.5	Roger RO4350B	High
This Work	**27.5 × 20**	**Single**	**30.26–34.15**	**10.97**	**9.83**	**31.3 GHz**	**30.6–34.15**	**30–31.55**	**FR4**	**Low**

6. Conclusion

A low-cost, compact wide-band *mm*–Wave concentric circle antenna is constructed using 3D electromagnetic simulation software. After that, a VNA and an anechoic chamber are used in a lab setting to test it. With this antenna, a broad bandwidth of 3.89 GHz (30.26–34.15GHz) and a high 5-dBi gain bandwidth of 2.50 GHz (30.47–32.97GHz) are achieved. The suggested structure exhibits a high degree of directivity of 12.76 dB at 31.3 GHz, although utilizing a substrate with a significant tangent loss (tan (δ) = 4.4). The frequency range of 30-31.59GHz has a mismatch loss of $\leq$ 0.044 dB, which guarantees a through power of $\geq$ 99% for this range. To improve 5–dBi-gain-bandwidth in the *mm*-Wave range, concentric circles are embedded into patch to divert the direction of current & a dumbbell-shaped slot is etched into the ground. Two semi-elliptical slots are etched at the upper edge of the GP, one on either side of the feeding line, to further diminish the coupling between the RRP & GP. The suggested design configuration arrangements are validated through the performance of parametric research. Based on performance metrics, this prototype may find use in intelligent network-based 5G and beyond next-generation communications, in *mm*–Wave range local multipoint distribution services (LMDS) 5G applications, and in futuristic robotic control devices.

References

[1] D. S. Wadhwa, P. K. Malik, and J. S. Khinda, "High gain antenna for n260-& n261-bands and augmentation in bandwidth for mm-wave range by patch current diversions," *World Journal of Engineering*, vol. 19, no. 5, pp. 689–696, 2022.

[2] J. S. Khinda, M. R. Tripathy, and D. Gambhir, "Multi-edged wide-band rectangular microstrip fractal antenna array for c-and x-band wireless applications," *Journal of Circuits, Systems and Computers*, vol. 26, no. 04, p. 1750068, 2017.

[3] S. K. Noor, N. Ramli, N. M. Sahar, and T. Khalifa, "Compact and wide bandwidth microstrip patch antenna for 5g millimeter wave technology: Design and analysis," in *Journal of Physics: Conference Series*, vol. 1878, no. 1. IOP Publishing, 2021, p. 012008.

[4] S. Singh, G. Sethi, and J. S. Khinda, "A historical development and futuristic trends of microstrip antennas," *International Journal of Computing and Digital Systems*, vol. 11, no. 1, pp. 187–204, 2022.

[5] C. A. Balanis, *Antenna theory: analysis and design*. John wiley & sons, 2015.

[6] D. S. Wadhwa, P. K. Malik, and J. S. Khinda, "mm-wave patch antenna for high data rate communication applications," in *2021 International Conference on Computing, Communication, and Intelligent Systems (ICCCIS)*. IEEE, 2021, pp. 778–781.

[7] J. S. Khinda, M. R. Tripathy, and D. Gambhir, "Improvement in depth of return loss of microstrip antenna for s-band applications," *Journal of Circuits, Systems and Computers*, vol. 27, no. 04, p. 1850058, 2018.

[8] D. S. Wadhwa and J. S. Malik, Praveen Kumar & Khinda, "Improvement in 5 dbi gain-bandwidth of wide band antenna for indoor k–, k a–band, millimeter-wave applications," *Journal of Infrared, Millimeter, and Terahertz Waves*, vol. 43, no. 7-8, pp. 527–549, 2022.

[9] H.-T. Hu and C. H. Chan, "Substrate-integrated-waveguide-fed wideband filtering antenna for millimeter-wave applications," *IEEE Transactions on Antennas and Propagation*, vol. 69, no. 12, pp. 8125–8135, 2021.

[10] C.-N. Hu, D.-C. Chang, C.-H. Yu, T.-W. Hsaio, and D.-P. Lin, "Millimeter-wave microstrip antenna array design and an adaptive algorithm for future 5g wireless communication systems," *International Journal of antennas and Propagation*, vol. 2016, 2016.

[11] S. F. Jilani, A. Rahimian, Y. Alfadhl, and A. Alomainy, "Low-profile flexible frequency-reconfigurable millimetre-wave antenna for 5g applications," *Flexible and Printed Electronics*, vol. 3, no. 3, p. 035003, 2018.

[12] M. M. S. Taheri, A. Abdipour, S. Zhang, and G. F. Pedersen, "Integrated millimeter-wave wideband end-fire 5g beam steerable array and low-frequency 4g lte antenna in mobile terminals," *IEEE Transactions on Vehicular Technology*, vol. 68, no. 4, pp. 4042–4046, 2019.

[13] D. Liu, X. Gu, C. W. Baks, and A. Valdes-Garcia, "Antenna-in-package design considerations for ka-band 5g communication applications," *IEEE Transactions on Antennas and Propagation*, vol. 65, no. 12, pp. 6372–6379, 2017.

[14] M. Mantash and T. Denidni, "Finger-worn end-fire antenna for mm-wave applications," *Microwave and Optical Technology Letters*, vol. 59, no. 10, pp. 2591–2593, 2017.

[15] S. Singh, G. Sethi, and J. S. Khinda, "Improvement in depth of reflection co-efficient below-20 db for millimeter–wave antenna," in *Journal of Physics: Conference Series*, vol. 2327, no. 1. IOP Publishing, 2022, p. 012048.

[16] A. Alsudani and H. M. Marhoon, "Design and enhancement of microstrip patch antenna utilizing mushroom like-ebg for 5g communications," *Journal of Communications*, vol. 18, no. 3, 2023.

[17] T. N. Cao, M. T. Nguyen, H. L. Phan, D. D. Nguyen, D. L. Vu, T. Q. H. Nguyen, J.-M. Kim *et al.*, "Millimeter-wave broadband mimo antenna using metasurfaces for 5g cellular networks," *International Journal of RF and Microwave Computer-Aided Engineering*, vol. 2023, 2023.

[18] A. Hamza, A. Chaabane, and H. Attia, "Gain improvement of wideband patch antenna at millimeter-wave band using novel metamaterial superstrate," in *2022 16th European Conference on Antennas and Propagation (EuCAP)*. IEEE, 2022, pp. 1–4.

[19] K. Gupta *et al.*, "Microstrip line and sloted lines, artech house norwood ma," 1996.

[20] T. C. Edward and M. B. Steer, "Foundation for microwave circuit design," *Wiley-EEE Press*, 1981.

[21] S. Y. Liao, *Microwave devices and circuits*. Pearson Education India, 2007.

[22] S. Singh, G. Sethi, and J. S. Khinda, "Low-loss uwb mm-wave monopole antenna using patch size enhancement for next-generation (5g and beyond) communications," *Journal of Infrared, Millimeter, and Terahertz Waves*, pp. 1–28, 2023.

Simerpreet Singh Simerpreet Singh received his B.E. degree in Instrumentation Engineering and Masters in Technology in Electrical Engineering. He is pursuing his Ph.D. in Electrical Engineering from Lovely Professional University, Punjab, India. His area of interest is wireless communication, Energy Harvesting and process control systems. Currently he is working as Assistant Professor in Department of Electrical Engineering Department in Bhai Gurdas Institute of Engineering and Technology affiliated to IKG Punjab Technical University, Jalandhar, and Punjab, India.

Gaurav Sethi Gaurav Sethi received his Ph.D. degree in Electronics & Communication Engineering from Dr B. R. Ambedkar National Institute of Technology Jalandhar in the area of Biomedical Image Processing. Presently, he is working as Professor in School of Electronics and electrical Engineering at Lovely Professional University, Phagwara, Punjab India. He has 14 years of rich experience of teaching & research and technical education management. His areas of interest are Digital Signal Processing, medical imaging, artificial Intelligence, Image Processing, healthcare services. He is the member of Indian Science Congress, Calcutta and Deputy Dean in Division of admissions.

Jaspal Singh Khinda Jaspal Singh Khinda earned his Ph.D. (2018) in Electronics and Communication Engineering at Amity School of Engineering and Technology, Amity University, NOIDA, Uttar Pradesh, India. He obtained a research Master's degree (2009) in Electronics and Communication Engineering in from the Punjab Technical University, Jalandhar, Punjab, India. He have 20 years rich experience in teaching, research and administration. Presently, he is working with Bhai Gurdas Institute of Engineering and Technology, Sangrur, Punjab, India as Professor in Electrical Department. His research interests include Ultra Wide–band, *mm*–Wave and re-configurable micro-strip Antennas. He also have filed 7–patents on wide band, *mm*–Wave micro-strip antenna. Dr. Khinda's primary research focus is steering major lobes of antenna using Python programming models for high-performance *mm*–Wave applications.